Available online at www.sciencedirect.com

ScienceDirect

Ceramics International 40 (2014) 3199–3207

CERAMICS INTERNATIONAL

www.elsevier.com/locate/ceramint

Growth of $(K_{0.5}Na_{0.5})NbO_3$–$SrTiO_3$ lead-free piezoelectric single crystals by the solid state crystal growth method and their characterization

Muhammad Umer Farooq, John G. Fisher*

School of Materials Science and Engineering, Chonnam National University, Gwangju 500-757, Republic of Korea

Received 4 September 2013; accepted 27 September 2013
Available online 7 October 2013

Abstract

Lead zirconate titanate (PZT) piezoelectric ceramics are commonly used in various applications, e.g. gas igniters, high-voltage generators and microbalances. However, due to increasing health and environmental concerns over their high lead content, lead-free piezoelectric ceramics are being developed. Lead-free piezoelectric single crystals offer superior performance over their polycrystalline counterparts but are difficult to grow by conventional methods. In this paper, $(K_{0.5}Na_{0.5})NbO_3$–$SrTiO_3$ (KNN–ST) single crystals are grown for the first time by the solid state crystal growth (SSCG) method. ⟨100⟩ $KTaO_3$ single crystal seeds are buried in the center of pellets of pressed KNN-ST powder. The single crystal grows from the seed crystal during sintering at 1100 °C for 20 h. The grown single crystals contain porosity, which is incorporated from the matrix during growth. The effect of $SrTiO_3$ addition on single crystal growth behavior, chemical composition and structure is evaluated.

Keywords: A. Grain growth; Lead free piezoelectric; Alkali niobates; Single crystal growth; Raman scattering

1. Introduction

Piezoelectric materials have the ability to convert electrical energy into mechanical energy and vice versa [1]. They have found a broad spectrum of applications, e.g. microelectromechanical systems (MEMS), ultrasonic baths, medical ultrasound imaging and scanning probe microscopes [2–4]. Lead zirconate titanate (PZT) based piezoelectric ceramics are commonly used for these applications because of their superior piezoelectric and dielectric performance [5]. However, PZT based ceramics contain a substantial amount of Pb. The high vapor pressure of PbO during production of PZT and Pb release from waste material contaminates the environment[6–8] and the toxicity of Pb is well documented [9]. Based on these environmental and health concerns, the European Union (EU) has limited or banned the use of Pb in many products [10]. If suitable alternatives to PZT based ceramics become available, the EU is expected to ban the use of PZT as well.

In the quest to find suitable replacements for PZT, many ceramic systems e.g. $(K_{0.5}Na_{0.5})NbO_3$ (KNN) [5,11,12], KNN with additions of $SrTiO_3$ (ST) [13] or $LiTaO_3$ [6], $(Na_{0.5}Bi_{0.5})TiO_3$–$BaTiO_3$ [14] and $BiFeO_3$–$BaTiO_3$ [15] have been explored. Among these systems, KNN-based materials are the most promising candidates. The $KNbO_3$-$NaNbO_3$ system is a pseudo-binary system with a morphotropic phase boundary between two orthorhombic phases close to the $(K_{0.5}Na_{0.5}NbO_3)$ composition [1]. KNN ceramics show reasonable piezoelectric and dielectric constants [16]. However, the performance of KNN ceramics is lower than that of PZT ceramics [5,17].

Various additions to KNN ceramics have been made to improve the dielectric and piezoelectric properties [6,7,16]. Previous reports on ST addition show improved dielectric constants and lower dielectric loss [7,13]. Addition of ST broadens the dielectric constant versus temperature peak, eventually changing the behavior from a normal ferroelectric ceramic to relaxor-like [4,18]. ST additions have also been found to improve the resistance to polarization switching fatigue and dielectric aging [4].

Polycrystalline piezoelectric ceramics have randomly oriented grains, meaning that the ferroelectric domains cannot be aligned perfectly in one direction during poling. This considerably deteriorates the properties of the material. In single crystals, a much improved alignment of the domains with the poling field

*Corresponding author. Tel.: +82 62 530 1702; fax: +82 62 530 1699.
E-mail address: johnfisher@jnu.ac.kr (J.G. Fisher).

0272-8842/$ - see front matter © 2013 Elsevier Ltd and Techna Group S.r.l. All rights reserved.
http://dx.doi.org/10.1016/j.ceramint.2013.09.122

can be achieved, leading to improved properties. Single crystals generally have better sensitivity and acoustic power, lower strain hysteresis, lower acoustic impedance and better efficiency when compared with polycrystalline piezoelectric ceramics [6,17,19]. Hence, the use of single crystals can boost the performance of lead-free systems and make them comparable to PZT [20].

Single crystals can be produced from a melt or flux [21,22] or by the solid state crystal growth (SSCG) method [8,19,23]. The SSCG method has many advantages over growth from a liquid. This method does not involve the melting of the starting materials, reduces contamination from the crucible walls and is particularly suitable for materials which melt incongruently [6]. Lower operating temperatures and the use of relatively inexpensive equipment make the SSCG method cost effective as well [2,19]. This method has been employed to grow single crystals of $BaTiO_3$ [23], $BaZrO_3$–$BaTiO_3$ [24] and $(Na_{0.5}Bi_{0.5})TiO_3$–$BaTiO_3$ [19].

Although single crystals of KNN [8] and KNN with $LiTaO_3$ [6] additions have been previously grown by SSCG, there are few reports on the single crystal growth of KNN-based ceramics by this method. In this paper, we present our work on the single crystal growth behavior of KNN-ST ceramics by the SSCG method for the first time. The effect of ST content on the single crystal and matrix grain growth is evaluated by microscopy. The effect of ST content on chemical composition and structure is evaluated by electron probe microanalysis and micro-Raman scattering.

2. Experimental

The $(1-x)[K_{0.5}Na_{0.5}NbO_3]-xSrTiO_3$ (x=0,1,2,3,4 mol%) powders, hereafter termed KNN(0–4)%ST, are produced by the solid state synthesis method. K_2CO_3 (Alfa Aesar, 99%), Na_2CO_3 (ACROS Organics, 99.5%), Nb_2O_5 (CEPA, 99.9%), $SrCO_3$ (Aldrich, 99.9%) and TiO_2 (Alfa Aesar, 99.8%) powders are used as starting materials. These powders are dried at 250 °C for 5 h to remove any adsorbed water. Then, weighed amounts of these powders are ball milled for 24 h in high-purity ethanol in polypropylene jars with ZrO_2 milling media. The ethanol is evaporated by using a hot plate with magnetic stirrer. The dried powder is ground using an agate mortar and pestle, and passed through a 180 μm mesh sieve to remove any agglomerates. The ground powder is placed in a high purity alumina crucible with lid and calcined in air at 850 °C for 5 h with heating and cooling rates of 5 °C/min. The calcined power is analyzed by X-ray diffraction (XRD, X'Pert PRO, PANalytical, Almelo, the Netherlands). All powders are single phase. Then, the powder is ball milled, ground and sieved again as before in order to remove any agglomerates that may have been formed during calcination.

$KTaO_3$ single crystals (MTI Corp, USA) with ⟨100⟩ orientation are used as seed crystals. A 3 mm × 3 mm × 0.5 mm seed crystal is buried in the center of 0.7 g powder in a steel die of 10 mm diameter. The powder is hand pressed, and the pellet is removed from the die. The pellet is then cold isostatically pressed (CIP) at 35 MPa pressure. The pellet is placed on a plate of sintered KNN in a high purity alumina crucible with lid and sintered in air at 1100 °C for 20 h with heating and cooling rates of 5 °C/min. The sintered pellet is vertically cut into two halves with a low speed diamond wheel saw, mounted in resin and polished to a 1 μm finish. One of the polished samples is thermally etched at 1050 °C for 1 h and Pt coated for scanning electron microscopy (SEM, Hitachi S-4700, Tokyo, Japan). The growth distance of the single crystals are measured from the micrographs. The grain size distribution is measured using ImageJ v1.46r image analysis software. The second polished sample is annealed at 500 °C for 1 h at a heating rate of 2 °C/min and cooling rate of 1 °C/min to remove any stresses generated during polishing. This sample is used for micro-Raman spectroscopy and electron probe micro analysis (EPMA). A LabRam HR800 UV (Horiba Jobin-Yvon, France) Raman microscope with 514 nm Ar^+ ion laser and 10 mW power is used for micro-Raman analysis at room temperature. The spectra were collected in backscattered geometry, with a resolution of ~0.5 cm^{-1} and a charge coupled device detector. The diameter of the laser spot on the sample is 1–2 μm. A Shimadzu JP/EPMA-1600 electron probe micro analyzer (Shimadzu, Kyoto, Japan) is used to evaluate the chemical composition and diffusion of seed crystal elements into the grown single crystal and matrix. The Wavelength Dispersive Spectroscopy (WDS) method is employed during EPMA analysis and KCl, NaCl, Nb metal, SrF_2, Ti metal and Ta metal are used as standards for K, Na, Nb, Sr, Ti and Ta, respectively. All the samples are carbon coated before EPMA analysis.

3. Results

Fig. 1 shows the grown single crystals in the KNN(0–4)% ST samples. A single crystal layer has grown on the seed crystal in the samples with 0–3 mol% $SrTiO_3$, but not in the sample with 4 mol% $SrTiO_3$. The single crystal growth distances are given in Fig. 2. Each data point is the mean value of 50 measurements and the error bars represent the standard deviation. The single crystal thickness initially increases with ST addition. The maximum thickness of the single crystal is ~97 μm with 2% ST solid solution addition. However, single crystal growth decreases rapidly at 3%ST addition and stops completely at 4% ST content. The single crystals contain pores of different sizes. Addition of 1% ST reduces the pore size, but 2% ST addition causes the pore size to increase again. 3% ST addition causes a large reduction in pore size. The pores are rectangular in shape and are aligned in the growth direction of the single crystal. The advancing face of the single crystal in the KNN sample is not flat, and the thickness of the single crystal layer varies between ~20 μm to ~40 μm. ST addition considerably reduces the variation in thickness of the single crystal layer. An exception is the KNN2%ST sample, which displays large variations in the thickness of the single crystal layer.

The chemical compositions of the samples are given in Table 1. Chemical analysis was not carried out on the KNN4%

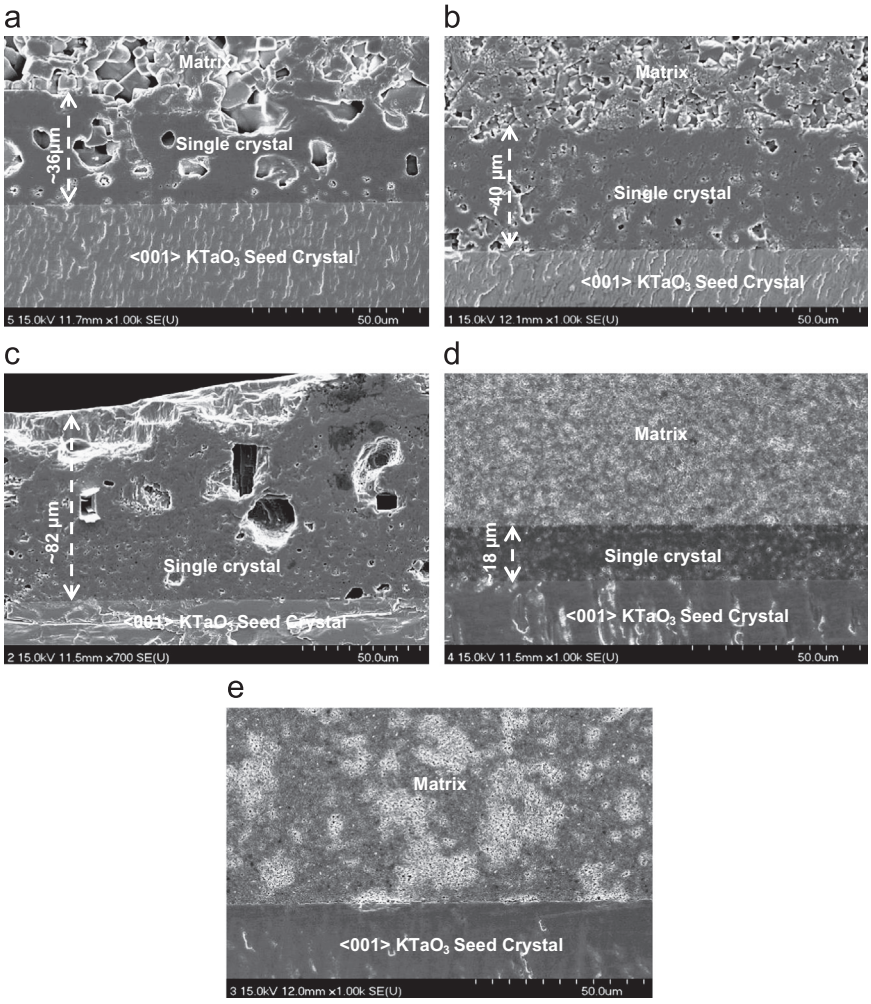

Fig. 1. SEM micrographs of grown single crystals of KNN-(0–4) mol% ST samples sintered at 1100 °C for 20 h. (a) 0%, (b) 1%, (c) 2%, (d) 3% and (e) 4%.

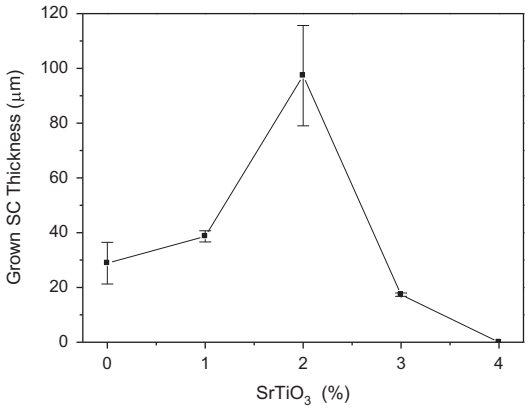

Fig. 2. Thickness of single crystals grown in KNN-(0–4) mol% ST samples sintered at 1100 °C for 20 h.

ST sample, as single crystal growth did not take place. The composition of the single crystal and the matrix in each sample is measured (three points for the single crystal and three points for the matrix) and each figure in the table represents the average value and standard deviation of these measurements. The composition is normalized to the nominal Nb concentration. The composition of the single crystal and the matrix is found to be similar to each other for all values of ST. The concentration of $SrTiO_3$ in the KNN2%ST and KNN3%ST samples is ~1 mol% lower than the nominal composition, indicating that there may be rejection of $SrTiO_3$ during growth of the single crystal. The composition of $SrTiO_3$ in the matrix grains is close to the nominal composition. The concentration of alkali elements is higher than the nominal concentration in all of the samples. Previous reports on KNN have pointed out the difficulty of accurate analysis of the alkali metal content by EDS analysis [6,25]. The Na Kα X-rays may be absorbed in the matrix and lead to lower concentration values [26]. However, this effect is less pronounced in the case of K and its concentration is closer to the nominal composition.[26] WDS analysis has been shown to give more accurate results than EDS when $KNbO_3$ and $NaNbO_3$ single crystals were used as standards [26]. The use of KCl and NaCl as standards in the present work may be the cause of the higher than expected alkali content.

Fig. 3 shows the concentration profile of Ta ions across the matrix, single crystal and seed crystal. This line spectrum is

Table 1
Chemical composition of ceramics measured by EPMA. All values are normalized to Nb concentration. SC=single crystal.

Element	KNN		KNN1%ST		KNN2%ST		KNN3%ST	
	SC	Matrix	SC	Matrix	SC	Matrix	SC	Matrix
K	0.545 ± 0.011	0.529 ± 0.019	0.568 ± 0.006	0.586 ± 0.020	0.531 ± 0.011	0.528 ± 0.010	0.596 ± 0.003	0.560 ± 0.017
Na	0.529 ± 0.017	0.561 ± 0.014	0.543 ± 0.009	0.468 ± 0.049	0.504 ± 0.007	0.517 ± 0.007	0.533 ± 0.005	0.507 ± 0.036
Nb	1.000 ± 0.000	1.000 ± 0.000	0.990 ± 0.000	0.990 ± 0.000	0.980 ± 0.000	0.980 ± 0.000	0.970 ± 0.000	0.970 ± 0.000
Sr	0.000 ± 0.000	0.000 ± 0.000	0.011 ± 0.001	0.012 ± 0.001	0.010 ± 0.007	0.021 ± 0.001	0.022 ± 0.001	0.033 ± 0.003
Ti	0.000 ± 0.000	0.000 ± 0.000	0.011 ± 0.0004	0.015 ± 0.003	0.012 ± 0.009	0.021 ± 0.000	0.034 ± 0.002	0.034 ± 0.002
Ta	0.006 ± 0.002	0.003 ± 0.002	0.001 ± 0.0002	0.001 ± 0.001	0.008 ± 0.006	0.002 ± 0.001	0.002 ± 0.001	0.002 ± 0.001

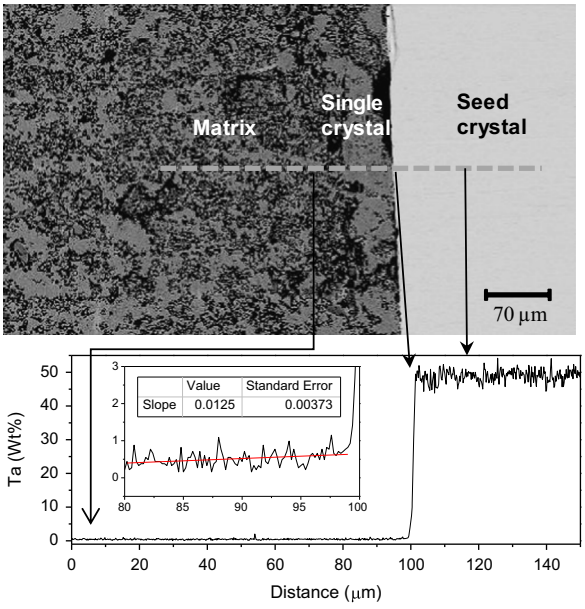

Fig. 3. EPMA Line spectrum for Ta concentration across the matrix, single crystal and seed crystal for the KNN1%ST sample. The inset graph shows the concentration in the region of the single crystal/seed crystal interface. The graph and inset graph have the same units.

obtained by EPMA for the KNN1%ST sample. The concentration of Ta is highest in the seed crystal as expected and decreases sharply from 50 wt% to < 1 wt% at the single crystal/seed-crystal interface, with a further decrease as the distance from the seed crystal increases.

Fig. 4 shows the matrix microstructure of the KNN(0–4)%ST samples. The grains show a cubic morphology with sharp facets, irrespective of ST content. This morphology is characteristic of KNN ceramics [25,27], which is retained after ST addition. Rectangular pores can be seen inside the grains. The facets of these pores are most probably low surface energy facets, perpendicular to the ⟨100⟩ direction as suggested by the presence of similar faceted pores in the single crystals in the current study and by Jenko et. al. in polycrystalline KNN ceramics [25]. The intragranular pore size decreases with the decrease in grain size. The KNN3%ST and KNN4%ST samples do not show intragranular pores, probably because of the submicron grain size of these ceramics (410 nm and 240 nm respectively). Intergranular pore size tends to decrease with the decreasing grain size as well. The mean grain size of the KNN(0–4)%ST samples is shown in Fig. 5. The grain size decreases with the addition of ST except for 2%ST addition were the grain size becomes anomalously large. The error bars are the standard deviation of the mean grain size and give an idea of the width of the grain size distribution. A wide distribution of the grain sizes is observed in the samples with 0–2%ST, but not in the samples with 3–4%ST.

Fig. 6 shows the Raman spectra of KNN-(0–3)%ST samples. The spectra of both single crystal and matrix are measured for each sample. The inset graph shows the Raman spectrum of the $KTaO_3$ seed crystal. The inset graph has same units and same scan range as that of the main graph. The seed crystal has the typical Raman spectrum for $KTaO_3$ [28]. The major peaks in the KNN spectra are the ν_1, ν_5 and $\nu_1+\nu_5$ combination modes [29]. It can be seen that the single crystal and matrix have similar spectra, which shows that the single crystal and matrix have similar structure and composition. These spectra are similar to already published work on KNN based ceramics [29,30]. The peak positions of the ν_1, ν_5 and $\nu_1+\nu_5$ combination modes are shown as a function of $SrTiO_3$ content in Fig. 7. The modes soften as ST concentration increases to 2%, then harden for the KNN-3%ST sample. There is a small difference in peak position between the single crystal and matrix in each sample.

4. Discussion

The growth of single crystals by SSCG is dependent upon the driving force for single crystal growth and upon the grain boundary structure of the ceramic, which determines whether normal or abnormal grain growth takes place. The driving force for growth of a grain in a polycrystalline matrix is given by [31,32]

$$\Delta\mu = \sigma\Omega\left(\frac{1}{\bar{r}} - \frac{1}{r}\right) \quad (1)$$

where σ is the average interfacial energy (grain boundary energy or solid / liquid interfacial energy), Ω the molar volume, r is the radius of the growing grain and $\bar{r}$ is the mean grain radius. The growing single crystal has a much larger radius than that of the matrix grains and so Eq. (1) can be

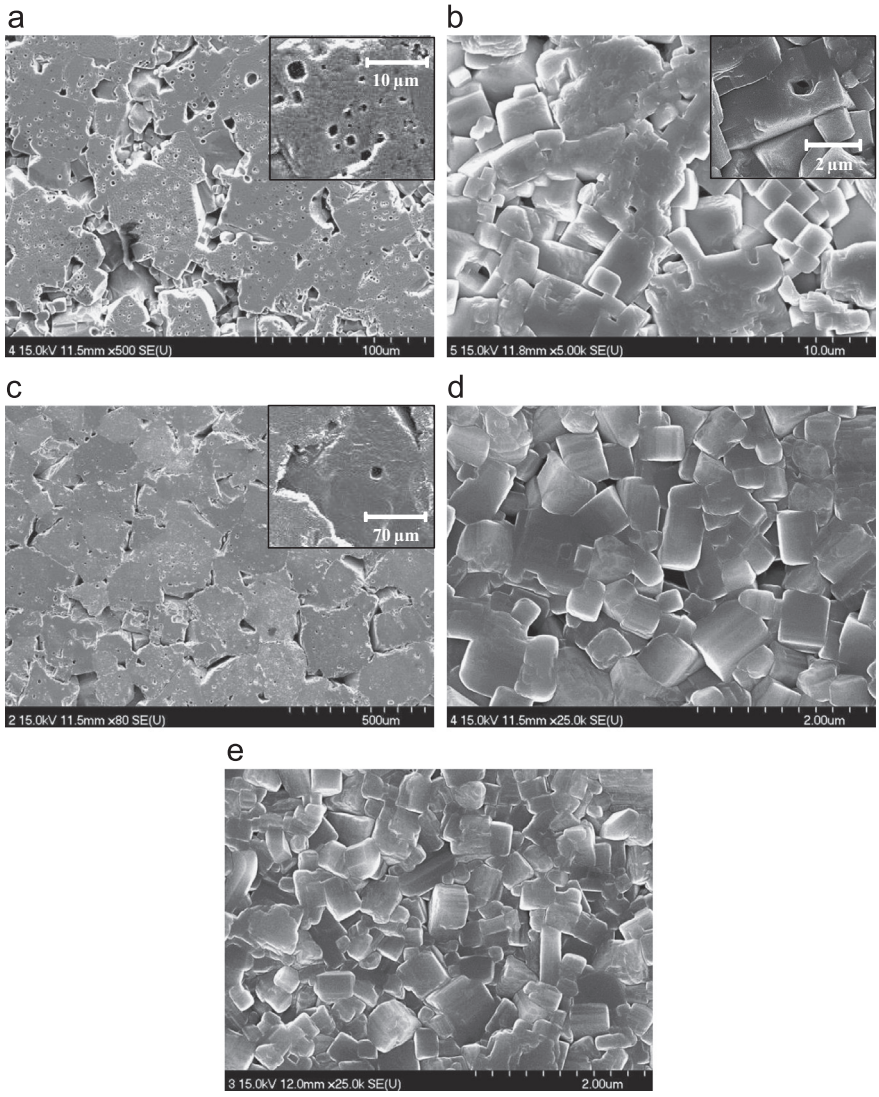

Fig. 4. SEM micrographs of KNN-(0–4)%ST samples sintered at 1100 °C for 20 h. (a) 0%, (b) 1%, (c) 2%, (d) 3% and (e) 4%. The insets show intragranular rectangular pores.

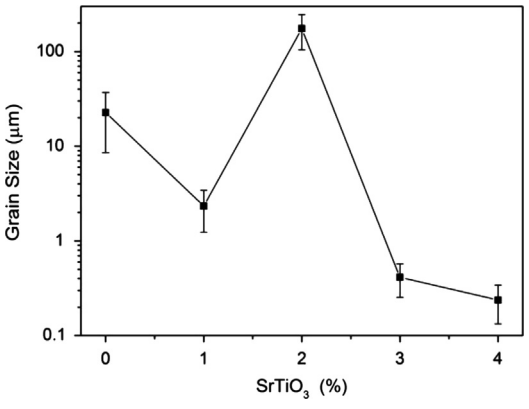

Fig. 5. The mean grain size of KNN-(0–4)%ST ceramics sintered at 1100 °C for 20 h.

approximated to:

$$\Delta\mu = \frac{\sigma\Omega}{\bar{r}} \quad (2)$$

The difference between the normal and abnormal grain growth mechanisms can be understood by considering the surface of the grains at an atomic level. If the grains have an atomically rough surface, the grain growth rate increases linearly with the driving force [33]. This is because atoms can attach to the growing grain at any place. Here, the growth rate is controlled by the rate of diffusion of atoms across the grain boundary. This situation is not favorable for single crystal growth [34].

In the case of an atomically flat or faceted surface, however, atoms cannot attach at any arbitrary point because of a large number of energetically unfavorable broken bonds. The only place for atoms to attach is at a ledge present on the surface of the growing grain. These ledges can be provided by screw dislocations [34], 2D nuclei [35] or twins [3]. Now, the growth rate is dependent on the availability of these ledges. The formation and growth of 2D nuclei is thermodynamically unstable if the driving force for grain growth is low. This places an energy barrier on the grain growth, and only grains

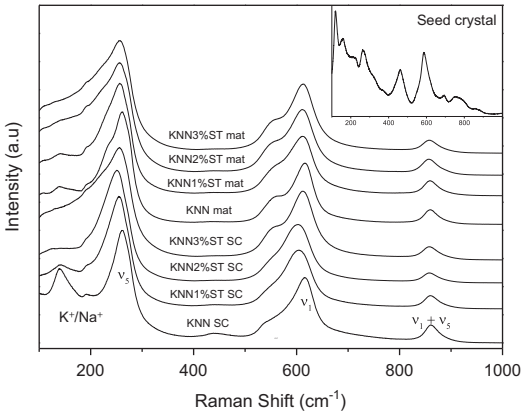

Fig. 6. Raman spectra of KNN-(0–3)%ST single crystal (SC) and matrix (mat). The inset graph shows the Raman spectrum of the $KTaO_3$ seed crystal. The graph and inset graph have same units.

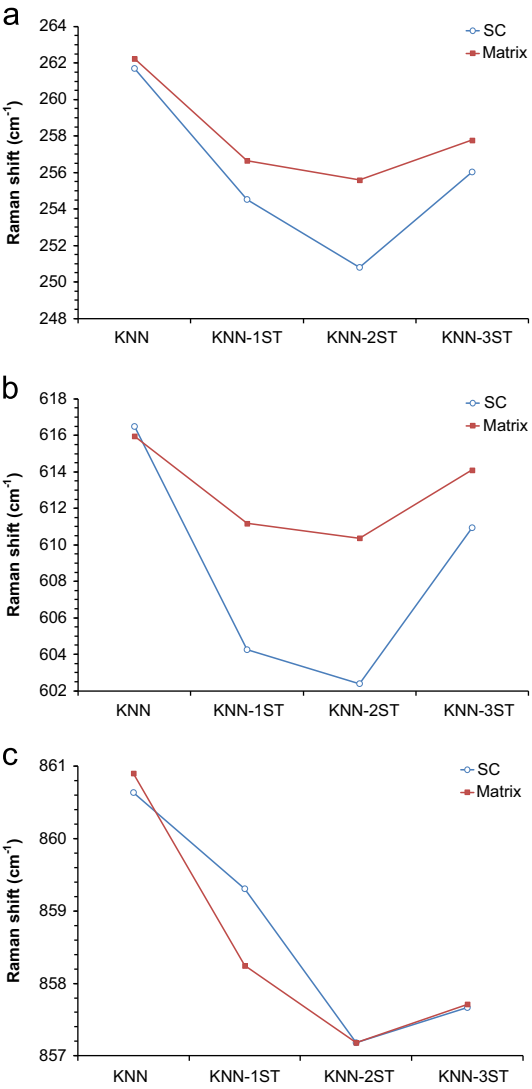

Fig. 7. Peak positions of the (a) ν_1 (b) ν_5 and (c) $\nu_1+\nu_5$ modes.

with a driving force higher than some critical value $\Delta\mu_C$ will grow. In this case, abnormal grain growth may take place. Most of the grains have driving forces for growth lower than $\Delta\mu_C$ and do not grow. Some grains will have driving forces higher than $\Delta\mu_C$ and can grow without hindrance to become large grains. Since KNN has faceted grains as shown in Fig. 4 and reported previously [25], abnormal grain growth is expected [8]. This abnormal grain growth plays the key role in single crystal growth by SSCG, as SSCG takes place via a mechanism in which abnormal growth is deliberately induced by and on the seed crystal [34]. For the KNN sample, both single crystal growth on the seed and abnormal grain growth in the matrix are observed (Figs. 1 and 4).

The effect of $SrTiO_3$ (ST) solid solution formation on the single crystal and grain growth behavior should now be considered. Formation of a solid solution with ST was previously observed to reduce the grain size of KNN [18]. Now, in this case, two opposite factors define the grown single crystal thickness. The smaller grain size enhances the driving force for single crystal growth (Eq. (2)), but if the ST content becomes too high, it will eventually retard both matrix grain and single crystal growth. The overall effect of these factors determines the final thickness of the single crystal. In the KNN sample, the mean grain size of the matrix is fairly large, so the single crystal growth is limited. Addition of 1% ST decreases the mean grain size, increasing the driving force for growth of the single crystal and the thickness of the single crystal increases. With 2% ST addition, the thickness of the single crystal increases considerably, implying an increased driving force for growth of the single crystal. A concomitantly small matrix grain size is expected; however, a very large grain size is also observed in the matrix. This could be the result of abnormal grain growth in the matrix as now the mean grain size is small enough to impose a large driving force for grain growth of any abnormal grains (Eq. (1)). As sufficient time is provided at high temperature, the abnormal grain growth has consumed all the small grains, and only large grains are left in the matrix. A systematic study with different time intervals for single crystal growth, which is underway, can further explain this phenomenon. When 3%ST is added, both matrix grain growth and single crystal growth are retarded and single crystal thickness decreases. With addition of 4% ST, grain size decreases further and single crystal growth is completely suppressed.

The variation in grown single crystal thickness in undoped KNN ceramics has been reported before by Fisher et al.[27] It may be due to local variations in the crystal growth rate caused by local variations in the matrix grain size at the crystal/matrix boundary. Formation of a solid solution with 1% and 3% ST reduces the width of the grain size distribution, reducing these local variations in crystal growth rate and leading to a smoother single crystal/matrix interface. The 2% ST sample is an exception, which may be due to the abnormal grain growth behavior of this sample.

When the single crystal grows, pores in the polycrystalline matrix can be picked up and dragged along by the single crystal / matrix interface [8,36]. If the mobility of the interface is higher than that of the pores, they will be left behind in the single crystal [37]. Pore coalescence and pore swelling in the matrix also takes place due to grain growth [38] and these larger pores are then incorporated into the growing single crystal. Some of the pores are rectangular in shape, with faces parallel

and perpendicular to the seed crystal face ⟨100⟩ as shown in Fig. 1. The faceted nature of the pores together with the faces parallel to the seed crystal face implies that the ⟨100⟩ direction, which makes the (100) plane face, has a lower surface energy than other plane faces. Similar results have been reported before for KNN [8,25] and $LiTaO_3$ doped KNN ceramics [6]. The intragranular pores in the matrix grains also have a rectangular shape (Fig. 4). Since the atomic arrangement in one grain is periodic, parallel faces must have similar surface energy. So, all the rectangular pores in one grain must have parallel facets if they are preferentially oriented to minimize the surface energy. This predicted behavior is observed in the microstructure as shown in the inset of Fig. 4(a).

During sintering, some diffusion of Ta from the seed into the KNN-ST lattice may take place. However, the results (Table 1 and Fig. 2) show that diffusion of Ta is minimal, as also found previously [8]. As well as diffusion from the seed into the single crystal, there may be diffusion from the single crystal into the seed crystal as well. It is confirmed by EPMA that the Na ions diffuse from the KNN-ST lattice into the seed lattice. The average concentration of Na in the seed crystal is approx. 0.016, when normalized to the Ta concentration. This is much higher than the amount of Ta present in the single crystal. The reason for the higher amount of Na^+ is probably its lower charge compared to Ta^{5+}, and its smaller size when compared to other A-site ions in the perovskite structure [18]. This would increase the diffusion rate of Na and its concentration in the seed.

Although there is a small amount of Ta diffusion from the seed to the single crystal, Nb does not show any diffusion from the single crystal into the seed. Both Nb^{+5} and Ta^{+5} carry the same charge and have the same ionic radii of 64 pm in 6-fold coordination with oxygen [18,39]. Therefore, both ions should show a similar diffusion rate, resulting in similar concentrations on opposite sides of the single crystal-seed interface. One possible explanation is that polarizability also plays an important role in the diffusion rate of an ion. Nb^{+5} is more polarizable than the Ta^{+5}, because of its lower atomic number [40]. When Nb enters a host lattice, it makes a stronger bond with oxygen than Ta does, and distorts the structure more severely than Ta. This will limit Nb substitution and lower the diffusion rate. The diffusion of Nb and Ta from the melt into Ta_2O_5–Nb_2O_5 ceramics and from haplogranite melt into rutile has shown this phenomenon [40,41]. The concentration of Nb was much lower than Ta in the solid in the aforementioned studies. Therefore, it is possible that the concentration of Nb in the seed crystal is lower than the Ta concentration in the single crystal, and even lower than the detection limit of the apparatus. A second possibility is the high formation energy of Nb vacancies in alkali niobates, which will limit the number of Nb ions which can leave the single crystal lattice to migrate into the seed crystal, as well as limiting Ta migration from the seed into the single crystal [42,43].

There is the possibility of Sr and Ti ion diffusion into the seed as well. Ti diffusion from the substrate into KNN thin films has been reported [44]. Since KNN-ST and the $KTaO_3$ seed share the perovskite structure, similar lattice parameter [45] and a similar size for the B-site cation (Ti 61 pm[18], Ta 64 pm [39]), Ti diffusion into the seed is expected. Sr^{+2} (144 pm) also has a similar ionic radius for the A-site K (164 pm) [18], but the charge is higher than K^{+1}. However, the Sr and Ti ion transport into the seed cannot be confirmed due to their low concentration in the single crystal, which would result in a very low concentration of these ions in the seed if diffusion happens at all.

In the Raman spectra of KNN-(0–3)%ST samples, shown in Fig. 6, the peaks are observed at around 260, 550, 610 and 860 cm^{-1}. All these modes are internal vibrational modes of NbO_6 octahedra. The ν_1 and ν_2 are stretching modes and ν_5 is a bending mode. The $\nu_1+\nu_5$ is the combination tone of ν_1 and ν_5 modes. The translational modes of K^{+1}/Na^{+1} versus NbO_6 octahedra are also observed at around 190 cm^{-1} and 150 cm^{-1}. Details of band assignments are available in published work [30,46]. The width of the peaks is broader in the KNN-ST samples in the present work when compared with KNN. In KNN-ST ceramics, Ti^{+4} partially replaces the Nb^{+5} at the B-site and Sr^{+2} partially replaces the K^{+1}/Na^{+1} at the A-site. This leads to disordering in the perovskite structure, which deforms the NbO_6 octahedra and lowers the local symmetry. The peak broadening is the result of this increased structural disorder [29]. The reduction in intensity of the peak at 150 cm^{-1} may be due to the partial replacement of K^+/Na^+ with Sr^{2+} ions. The softening of the ν_1, ν_5 and $\nu_1+\nu_5$ modes may be attributed to the decrease in the bond length of O–Nb–O due to incorporation of Ti^{+4} replacing the Nb^{+5} [29,30]. The mode softening may also be due to the approach of a polymorphic phase transition between orthorhombic and tetragonal phases [47]. The difference in peak positions between the single crystal and the matrix in each sample may be due to differences in crystallographic orientation [46].

5. Conclusions

Single crystals of $(1-x)[K_{0.5}Na_{0.5}NbO_3]$-x$SrTiO_3$ (x=0,1,2,3 mol%) are grown for the first time by the solid state crystal growth (SSCG) method. A ⟨001⟩ oriented $KTaO_3$ single crystal is used as a seed to grow KNN-ST single crystals. $SrTiO_3$ solid solution addition reduces the grain size and increases the driving force for single crystal growth. The grown single crystal thickness increases with the $SrTiO_3$ content, reaches a maximum of 97 μm with 2% $SrTiO_3$ addition, and then declines. The falloff in single crystal thickness can be attributed to the higher $SrTiO_3$ content, which hinders both matrix and single crystal growth. This effect is so pronounced with 4% $SrTiO_3$ addition that the single crystal growth stops altogether. EPMA analysis indicates a rejection of $SrTiO_3$ from the growing crystals in the samples with 2 and 3% $SrTiO_3$ addition. For all samples, a small amount of diffused Ta from the seed crystal is detected in the single crystal. A relatively higher amount of diffused Na from the single crystal is observed in the seed crystal. Raman spectroscopy reveals the similar structure of the grown single crystal and matrix. The peak shift towards lower wavenumbers and peak broadening in KNN-ST ceramics can be attributed to

the $SrTiO_3$ addition, which decreases the bond lengths of NbO_6 octahedra, decreases the structural order and lowers the orthorhombic-tetragonal transition temperature.

Acknowledgments

This work was funded by the National Research Foundation of Korea (Ministry of Education, Science and Technology, project no. 2012R1A1A2000925). The authors would like to thank Dr. Sang-Hun Jeong (Korea Basic Science Institute, Gwangju center) for carrying out the micro-Raman scattering experiments, and Cheol Kim, Chan Yoon and Hye-Jeong Kim for operating the XRD, EPMA and SEM respectively.

References

[1] B. Jaffe, W.R. Cook, H. Jaffe, Piezoelectric Ceramics, Academic press, London, 1971.
[2] Z.-G. Ye, Handbook of Advanced Dielectric, Piezoelectric and Ferroelectric Materials: Synthesis, Properties and Applications, CRC Press, Cambridge, 2008.
[3] B.-K. Lee, S.-Y. Chung, S.-J.L. Kang, Grain boundary faceting and abnormal grain growth in $BaTiO_3$, Acta Materialia 48 (7) (2000) 1575–1580.
[4] V. Bobnar, J. Bernard, M. Kosec, Relaxor-like dielectric properties and history dependent effects in a new lead-free $K_{0.5}Na_{0.5}NbO_3$–$SrTiO_3$ ceramic system, Applied Physics Letters 85 (6) (2004) 994–996.
[5] F. Rubio-Marcos, A. Del Campo, R. López-Juárez, J.J. Romero, J.F. Fernández, High spatial resolution structure of (K,Na)NbO_3 lead-free ferroelectric domains, Journal of Materials Chemistry 22 (19) (2012) 9714.
[6] J.G. Fisher, A. Benčan, J. Bernard, J. Holc, M. Kosec, S. Vernay, D. Rytz, Growth of (Na, K, Li)(Nb, Ta)O_3 single crystals by solid state crystal growth, Journal of the European Ceramic Society 27 (13–15) (2007) 4103–4106.
[7] R.-C. Chang, S.-Y. Chu, Y.-P. Wong, C.-S. Hong, H.-H. Huang, The effects of sintering temperature on the properties of lead-free $(Na_{0.5}K_{0.5})NbO_3$–$SrTiO_3$ ceramics, Journal of Alloys and Compounds 456 (1–2) (2008) 308–312.
[8] J.G. Fisher, A. Benčan, J. Holc, M. Kosec, S. Vernay, D. Rytz, Growth of potassium sodium niobate single crystals by solid state crystal growth, Journal of Crystal Growth 303 (2) (2007) 487–492.
[9] U. ATSDR, Toxicological profile for lead, US Department of Health and Human Services (2007) 1–582.
[10] E. Directive, Directive 2002/95/EC of the European Parliament and of the Council of 27 January 2003 on the restriction of the use of certain hazardous substances in electrical and electronic equipment, Official Journal of the European Union 13 (2003) L37.
[11] J.G. Fisher, S.-Y. Choi, S.-J.L. Kang, Influence of sintering atmosphere on abnormal grain growth behaviour in potassium sodium niobate ceramics sintered at low temperature, Journal of the Korean Ceramic Society 48 (6) (2011) 641–647.
[12] J.G. Fisher, S.-J.L. Kang, Microstructural changes in $(K_{0.5}Na_{0.5})NbO_3$ ceramics sintered in various atmospheres, Journal of the European Ceramic Society 29 (12) (2009) 2581–2588.
[13] Y. Guo, K.-i. Kakimoto, H. Ohsato, Dielectric and piezoelectric properties of lead-free $(Na_{0.5}K_{0.5})NbO_3$–$SrTiO_3$ ceramics, Solid State Communications 129 (5) (2004) 279–284.
[14] T. Takenaka, K.-I. Maruyama, K. Sakata, $(Bi_{1/2}Na_{1/2})$ $TiO_3-BaTiO_3$ system for lead-free piezoelectric ceramics, Japanese Journal of Applied Physics 30 (9B) (1991) 2236–2239.
[15] H. Yang, C. Zhou, X. Liu, Q. Zhou, G. Chen, W. Li, H. Wang, Piezoelectric properties and temperature stabilities of Mn- and Cu-modified $BiFeO_3$–$BaTiO_3$ high temperature ceramics, Journal of the European Ceramic Society 33 (6) (2013) 1177–1183.
[16] Y. Chang, Z. Yang, X. Chao, R. Zhang, X. Li, Dielectric and piezoelectric properties of alkaline-earth titanate doped $(K_{0.5}Na_{0.5})NbO_3$ ceramics, Materials Letters 61 (3) (2007) 785–789.
[17] J. Rödel, W. Jo, K.T.P. Seifert, E.-M. Anton, T. Granzow, D. Damjanovic, Perspective on the development of lead-free piezoceramics, Journal of the American Ceramic Society 92 (6) (2009) 1153–1177.
[18] R.-C. Chang, S.-Y. Chu, Y.-P. Wong, Y.-F. Lin, C.-S. Hong, Properties of $(Na_{0.5}K_{0.5})NbO_3$–$SrTiO_3$ based lead-free ceramics and surface acoustic wave devices, Sensors and Actuators A: Physical 136 (1) (2007) 267–272.
[19] K.-S. Moon, D. Rout, H.-Y. Lee, S.-J.L. Kang, Solid state growth of $Na_{1/2}Bi_{1/2}TiO_3$–$BaTiO_3$ single crystals and their enhanced piezoelectric properties, Journal of Crystal Growth 317 (1) (2011) 28–31.
[20] M. Davis, N. Klein, D. Damjanovic, N. Setter, A. Gross, V. Wesemann, S. Vernay, D. Rytz, Large and stable thickness coupling coefficients of $[001]_C$-oriented $KNbO_3$ and Li-modified (K,Na)NbO_3 single crystals, Applied Physics Letters 90 (6) (2007) (062904-062904-062903).
[21] J.C. Wu, Z.B. Chen, R.K. Choubey, C.W. Lan, On the study of zinc doping in congruent LiTaO3 crystals, Materials Chemistry and Physics 133 (2–3) (2012) 813–817.
[22] R. Sun, X. Li, Q. Zhang, B. Fang, H. Zhang, D. Lin, S. Wang, X. Zhao, H. Luo, Growth and electrical properties of $0.95Na_{0.5}Bi_{0.5}TiO_3$–$0.05K_{0.5}Bi_{0.5}TiO_3$ lead-free piezoelectric crystal by the TSSG method, Journal of Crystal Growth 341 (1) (2012) 34–37.
[23] P.W. Rehrig, G.L. Messing, S. Trolier-McKinstry, Templated grain growth of barium titanate single crystals, Journal of the American Ceramic Society 83 (11) (2000) 2654–2660.
[24] P.W. Rehrig, S.-E. Park, S. Trolier-McKinstry, G.L. Messing, B. Jones, T.R. Shrout, Piezoelectric properties of zirconium-doped barium titanate single crystals grown by templated grain growth, Journal of Applied Physics 86 (3) (1999) 1657–1661.
[25] D. Jenko, A. Bencan, B. Malic, J. Holc, M. Kosec, Electron microscopy studies of potassium sodium niobate ceramics, Microscopy and Microanalysis 11 (6) (2005) 572–580.
[26] Z. Samardžija, S. Bernik, R.B. Marinenko, B. Malič, M. Čeh, An EPMA study on $KNbO_3$ and $NaNbO_3$ single crystals–potential reference materials for quantitative microanalysis, Microchimica Acta 145 (1–4) (2004) 203–208.
[27] J.G. Fisher, A. Benčan, J. Godnjavec, M. Kosec, Growth behaviour of potassium sodium niobate single crystals grown by solid-state crystal growth using $K_4CuNb_8O_{23}$ as a sintering aid, Journal of the European Ceramic Society 28 (8) (2008) 1657–1663.
[28] S. Glinsek, D. Nuzhnyy, J. Petzelt, B. MaliC, S. Kamba, V. Bovtun, M. Kempa, V. Skoromets, P. Kuzel, I. Gregora, M. Kosec, Lattice dynamics and broad-band dielectric properties of the $KTaO_3$ ceramics, Journal of Applied Physics 111 (10) (2012) 104101.
[29] M. Połomska, B. Hilczer, M. Kosec, B. Malič, Raman scattering studies of lead free $(1-x)K_{0.5}Na_{0.5}NbO_{3-x}SrTiO_3$ relaxors, Ferroelectrics 369 (1) (2008) 149–156.
[30] K.-i. Kakimoto, K. Akao, Y. Guo, H. Ohsato, Raman scattering study of piezoelectric $(Na_{0.5}K_{0.5})$ NbO3_LiNbO$_3$ ceramics, Japanese Journal of Applied Physics 44 (2005) 7064.
[31] Y.J. Park, N.M. Hwang, D.Y. Yoon, Abnormal growth of faceted (WC) grains in a (Co) liquid matrix, Metallurgical and Materials Transactions A 27 (9) (1996) 2809–2819.
[32] H.I. Yoo, S.J.L. Kang, in: The Step Growth Hypothesis for Abnormal Grain Growth. In Ceramic Interfaces 2, Institute of Materials, London, 2001.
[33] I.M. Lifshitz, V.V. Slyozov, The kinetics of precipitation from supersaturated solid solutions, Journal of Physics and Chemistry of Solids 19 (1) (1961) 35–50.
[34] S.-Y. Chung, D.Y. Yoon, S.-J.L. Kang, Effects of donor concentration and oxygen partial pressure on interface morphology and grain growth behavior in $SrTiO_3$, Acta Materialia 50 (13) (2002) 3361–3371.
[35] C.W. Park, D.Y. Yoon, Effects of SiO_2, CaO_2, and MgO additions on the grain growth of alumina, Journal of the American Ceramic Society 83 (10) (2000) 2605–2609.
[36] Y.M. Chiang, D. Birnie, W.D. Kingery, Physical Ceramics: Principles for Ceramic Science and Engineering, John Wiley & Sons, New York, 1997.

[37] S.-J.L. Kang, Sintering: Densification, Grain Growth & Microstructure, Elsevier, Butterworth Heineman, Oxford, 2005.
[38] U.C. OH, Y.S. CHUNG, D.Y. KIM, D.N. YOON, Effect of grain growth on pore coalescence during the liquid-phase sintering of MgO–CaMg-SiO_4 systems, Journal of the American Ceramic Society 71 (10) (1988) 854–857.
[39] X. Wu, Z. Wen, X. Wang, X. Xu, J. Lin, S. Song, Effect of Ta-doping on the ionic conductivity of lithium titanate, Fusion Engineering and Design 85 (7–9) (2010) 1442–1445.
[40] W.-S. Horng, P.C. Hess, Partition coefficients of Nb and Ta between rutile and anhydrous haplogranite melts, Contributions to Mineralogy and Petrology 138 (2) (2000) 176–185.
[41] M.W. Schmidt, A. Dardon, G. Chazot, R. Vannucci, The dependence of Nb and Ta rutile–melt partitioning on melt composition and Nb/Ta fractionation during subduction processes, Earth and Planetary Science Letters 226 (3–4) (2004) 415–432.
[42] A. Shigemi, T. Wada, Enthalpy of formation of various phases and formation energy of point defects in perovskite-type $NaNbO_3$ by first-principles calculation, Japanese Journal of Applied Physics 43 (2004) 6793.
[43] A. Shigemi, T. Wada, Evaluations of phases and vacancy formation energies in $KNbO_3$ by first-principles calculation, Japanese Journal of Applied Physics 44 (2005) 8048.
[44] P.C. Goh, K. Yao, Z. Chen, Titanium diffusion into $(K_{0.5}Na_{0.5})NbO_3$ thin films deposited on Pt/Ti/SiO2/Si substrates and corresponding effects, Journal of the American Ceramic Society 92 (6) (2009) 1322–1327.
[45] A. Bencan, E. Tchernychova, M. Godec, J. Fisher, M. Kosec, Compositional and structural study of a $(K_{0.5}Na_{0.5})NbO_3$ single crystal prepared by solid state crystal growth, Microscopy and Microanalysis 15 (5) (2009) 435–440.
[46] W. Zhu, J. Zhu, M. Wang, B. Zhu, X. Zhu, G. Pezzotti, Raman tensor analysis of $(K_{0.5}Na_{0.5})NbO_3$–$LiSbO_3$ lead-free ceramics and its application to study grain/domain orientation, Journal of Raman Spectroscopy 43 (2012) 1320–1328.
[47] J.G. Fisher, D. Rout, K.-S. Moon, S.-J.L. Kang, High-temperature X-ray diffraction and Raman spectroscopy study of $(K_{0.5}Na_{0.5})NbO_3$ ceramics sintered in oxidizing and reducing atmospheres, Materials Chemistry and Physics 120 (2–3) (2010) 263–271.